Thermal Decomposition of Hydrated Graphite Oxide: A Computational Study

Andrii Kyrylchuk,[1] Pranav Surabhi,[2] and David Tománek[3,*]

[1] *Institute of Organic Chemistry, National Academy of Sciences of Ukraine, Murmanska Street 5, Kyiv, 02660, Ukraine*

[2] *Indian Institute of Technology, Khandwa Road, Simrol, Indore, 453552, India*

[3] *Physics and Astronomy Department, Michigan State University, East Lansing, Michigan 48824, USA*

(Received 29 October 2021; accepted 3 March 2022; published 7 April 2022)

We study the behavior of hydrated graphite oxide (GO) at high temperatures using thermally-accelerated molecular dynamics simulations based on *ab initio* density-functional theory. Our results suggest that GO, a viable candidate for water treatment and desalination membranes, is more heat resilient than currently used organic materials. The system we consider to represent important aspects of thermal processes in highly disordered GO is a hydrated GO bilayer in a vacuum. Our study provides microscopic insight into reactions involving water and functional epoxy-O and OH groups bonded to graphene layers, and also describes the swelling of the structure by water vapor pressure at elevated temperatures. We find the system withstands simulation temperatures up to approximately 2500 K before the graphitic layers start decomposing, implying the possibility of cleaning biofouling residue from a GO-based membrane by heating it in an inert-gas atmosphere.

DOI: 10.1103/PhysRevApplied.17.044015

I. INTRODUCTION

Lack of potable water is the most-urgent problem facing humankind today. Although water in oceans is plentiful, it requires desalination before human consumption [1]. The most-common desalination process is reverse osmosis [2]. The key component of a reverse-osmosis desalination plant is a strong semipermeable membrane that lets water molecules pass through it but rejects ions. Current membranes, based on polyamide and other organic nanoporous substances, exhibit satisfactory ion rejection at acceptable water-permeation rates [3], implying that new materials should offer only marginal improvement in performance [4]; however, these optimized membranes have serious limitations in their mechanical, thermal, and chemical stability [5]. An urgent problem in all water treatment is the formation of a biofouling residue that clogs the membrane [5,6]. Cleaning this residue with chemical agents is of limited use for organic membranes, since such chemicals also attack the membrane material [7,8]. The desalination community has long been waiting for a paradigm shift that alleviates this problem [9,10].

Here we present results of an *ab initio* density-functional theory (DFT) molecular dynamics (MD) simulation addressing thermally driven structural changes in a bilayer of hydrated graphite oxide (GO) in a vacuum. This rather artificial system is selected as a model to study microscopic details of the thermal decomposition of GO, which has been demonstrated to allow water permeation while rejecting solvated ions in the feed [11] when sandwiched in-between layers of carbon-nanotube buckypaper and carbon fabric for containment and mechanical strength [12]. To observe slow processes in the short time frame of the simulation, we artificially raise the system temperature in our thermally-accelerated MD studies [13]. At simulation temperatures up to 4000 K, we find that water molecules in the interlayer region are rather decoupled from the GO layers and only marginally affect their behavior except for swelling the structure by water vapor pressure. In the presence of nearby water molecules, some epoxy-O atoms move from their bridge to the on-top site, turning into radicals and changing the configuration of the connected carbon atom from sp^3 to sp^2. In a similar way, in the presence of water, hydrogen atoms often detach from adsorbed hydroxy groups and turn them into epoxy groups. Both processes facilitate buckling and local fracture of the graphitic backbone above 2500 K. At higher temperatures, we observe the destruction of the graphitic backbone itself. Oxygen atoms in the functional groups migrate from the faces to the reactive exposed edges of the graphitic flakes, turning GO into hydrophobic reduced GO (rGO), which is not subject to swelling.

As indicated above, the vast majority of state-of-the-art desalination membranes use nanoporous organic compounds in the active layer. Yet as early as 1961, Boehm [11] reported that GO [14,15], an inorganic compound

*tomanek@msu.edu

related to graphite, is impermeable with regard to liquids other than polar water. The same study [11] found that GO is practically impermeable with regard to anions but permeable with regard to cations. With a few notable exceptions [16,17], the reported selectivity and permeation by water were barely noticed by the membrane community, since GO is essentially a disordered powder that is hard to characterize and to contain.

GO has undergone serious characterization analysis by experimental and theoretical techniques since its discovery and the development of effective synthesis techniques [14,15]. The basic conclusion is that GO partly resembles what we now know as intercalated graphite, by containing finite-sized graphene flakes, functionalized mainly by O and OH groups, which are largely disordered and separated by water molecules [18]. Progress has also been made in improving flake alignment within this layered system [19]. Interestingly, the presence of thermally stable and electrically conductive graphitic material has been observed to reduce biofouling in membranes [20–29].

Whereas advanced experimental techniques have provided a significant amount of structural and chemical information, microscopic knowledge of atomic-level processes in GO is scarce due to its complex structure and disorder, which changes in the presence of water. Probably the best description of swelling and thermal reduction of GO to rGO to date is provided in the 1934 study by Hofmann [18].

Computer simulations of this complex, disordered system are seriously limited by the total simulation time and the size of the system, where the quantum nature of interatomic interactions is essential for a correct prediction of atomic-scale processes. Thus, atomic-level studies of a substance as complex as hydrated GO are possible only in a model system that is much simpler, yet closely represents at least one of its aspects. Finding such an ideal model system in nature is almost impossible. Theory, on the other hand, deals with simplified model systems, primarily to obtain an understanding of ongoing atomic-level processes. Such studies then provide useful information for only a limited number of phenomena observed in the more-complex GO system.

Related theoretical studies have considered water flow in-between GO layers [30,31] and inside carbon nanotubes [32,33]. Most important for selective permeation by water and rejection of ions were model studies of in-layer pores within GO monolayers [12]. A pore consisting of a pair of in-layer GO edges was characterized by the pore width, the edge type being either armchair or zigzag, and termination by H, O, or OH groups. The results of that study indicated that selective permeation by water and rejection of ions is possible for pores not narrower than 0.7 nm and not wider than 0.9 nm, in agreement with the consensus in the water-treatment community [3].

Thermal stability of GO and its disintegration at high temperatures has been investigated theoretically in only a few studies [34]. Yet the behavior of GO at elevated temperatures is the key to answering the question of whether GO membranes may be cleaned by heating, possibly in an inert-gas atmosphere. A MD study of a model system at elevated temperatures may reveal if OH and O functional groups, which lower the mechanical strength of GO, remain attached up to the temperature when C—C bonds break, and thus induce the disintegration of the graphitic backbone. A MD study should also reveal if interlayer water turned to vapor may exert sufficient pressure to separate adjacent GO layers, and whether water molecules may exchange atoms and modify the structure of functional groups.

Theory has the unique advantage of describing a hypothetical system that should exist but is nearly impossible to synthesize. The single purpose of such a system is to study particular aspects of behavior that would be hard to isolate in a more-complex system. The specific system we address in this study is an infinite, defect-free bilayer of graphite oxide, suspended in a vacuum, which contains water molecules in the interlayer region in much the same way as the bulk system does. This geometry also offers the benefit of not suppressing changes in the interlayer separation by artificial boundary conditions.

II. COMPUTATIONAL APPROACH

Our computational approach to study hydrated GO is based on *ab initio* DFT as implemented in the SIESTA [35] code. We use the nonlocal Perdew-Burke-Ernzerhof (PBE) [36] exchange-correlation functional in the SIESTA code, norm-conserving Troullier-Martins pseudopotentials [37], a double-ζ basis including polarization orbitals, and a mesh cutoff energy of 180 Ry to determine the self-consistent charge density. The hydrated bilayer of graphite oxide, described by the Lerf-Klinowski model [38], is shown in Fig. 1. Of the 308 atoms in the unit cell, there are 96 carbon atoms in the two graphitic layers and 44 H_2O molecules in the interlayer region. The remaining 32 H and 48 O atoms form epoxy-O and OH functional groups covalently bonded to the graphene layer. We use periodic boundary conditions throughout the study, with replicas of the bilayer initially separated by a large distance of 30 Å. While computationally rather demanding, the DFT PBE energy functional is free of adjustable parameters and has been used extensively to provide an unbiased description of water and its interaction with solids [39,40].

Slow chemical processes pose a significant challenge to atomistic MD simulations, which we use. Yet according to a well-known chemical rule of thumb, the speed of a reaction doubles on a temperature increase of 10 K. The high computational cost of the *ab initio* force field and the large size of the unit cell limit our calculations to approximately

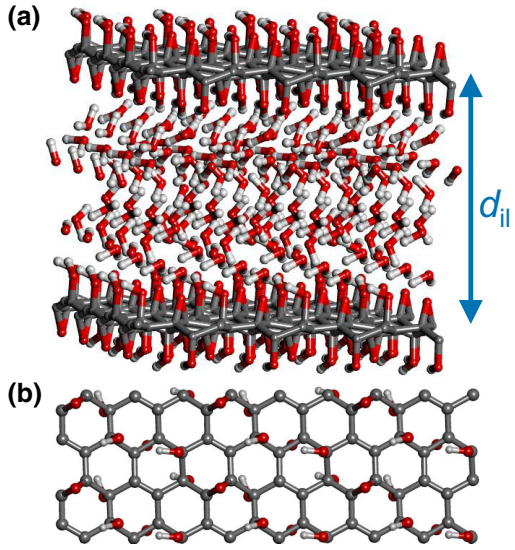

FIG. 1. Ball-and-stick models of a GO bilayer containing H_2O molecules in the interlayer region. (a) A 2 × 2 GO bilayer supercell in perspective view. d_{il} is the interlayer distance. (b) The top layer in top view displaying O atoms forming 1,3-epoxy groups and OH groups chemisorbed on the graphene layer.

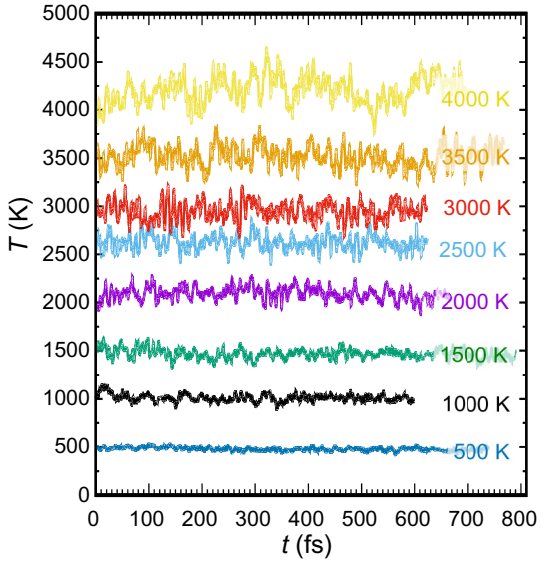

FIG. 2. Temperature fluctuations during an *NVE* simulation of the hydrated-GO-bilayer unit cell containing 308 atoms. The temperatures at which each ensemble is initialized are indicated by the labels and are discussed in the main text.

1 ps or less. To observe processes that occur in nature on the timescale of seconds, within the short period of 1 ps, chemical processes have to be accelerated by a factor of 10^{12}. This may be achieved using an approach we call "thermally accelerated dynamics." If we take the above-mentioned chemical rule of thumb seriously, to at least 1 order of magnitude, a desirable acceleration should occur once the temperature of the system has been raised artificially by $\Delta T \approx 200$–2000 K. Consequently, processes occurring during less than 1 ps at the simulation temperature T are expected to occur at a much lower temperature $T - \Delta T$ in nature on the timescale of seconds or longer.

We select simulation temperatures in the range from 500 to 4000 K to initially equilibrate the system for a period of 60 fs by treating it as a canonical (*NVT*) ensemble regulated by a Nosé thermostat. Following this equilibration period, the system is treated as a microcanonical (*NVE*) ensemble to avoid artifacts caused by the thermostat. We find that 0.3-fs time steps are sufficiently short to keep the total energy in the *NVE* ensemble conserved, while allowing the temperature to fluctuate, as seen in Fig. 2. As expected, the temperature fluctuations increase with system temperature T. In view of the relatively large unit-cell size, the range of temperature fluctuations in the *NVE* ensemble is adequate and should not affect our conclusions.

III. RESULTS

Our MD results depicting the behavior of a hydrated-GO monolayer at $T = 500$ K are presented in Video 1. The reason for GO being hydrophilic is that the calculated adsorption energy of 0.73 eV of an isolated H_2O molecule on GO exceeds its calculated hydration energy of 0.41 eV. Still, this energy is rather low, so molecules surrounding the monolayer detach easily and evaporate into the vacuum region above and below even on the short timescale below 1 ps at 500 K.

As mentioned before, we consider a bilayer with water contained in the interlayer region to keep GO hydrated. Since water molecules detach easily above the top layer and below the bottom layer, they do not affect the dynamics of the bilayer and are omitted in our simulations. In our periodic system, infinite hydrated bilayers are separated by a substantial vacuum region that eliminates the interaction between replicas even under the most-extreme conditions.

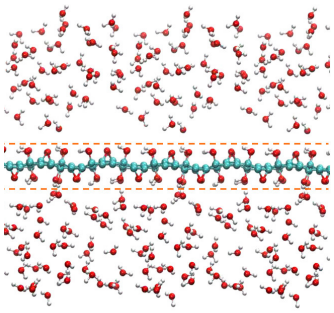

VIDEO 1. Microcanonical MD simulation of a hydrated-GO monolayer that is initially equilibrated at $T = 500$ K, visualizing the slow detachment of adsorbed water from both sides. A 3 × 3 × 1 supercell is shown for clarity.

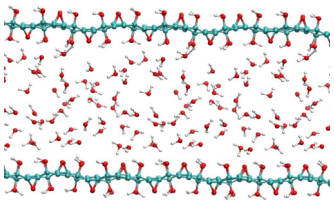

VIDEO 2. Microcanonical MD simulation of a hydrated-GO bilayer that is initially equilibrated at $T = 500$ K. A $3 \times 3 \times 1$ supercell is shown for clarity.

In this geometry, all atoms in the bilayer are completely free to move rather than being constrained in the out-of-plane direction as they would be in bulk GO with imposed periodicity in that direction.

A. Atomic motion at elevated temperatures

The results of our MD simulations for the hydrated-GO bilayer are shown in Video 2 for $T = 500$ K, in Video 3 for $T = 1000$ K, in Video 4 for $T = 1500$ K, in Video 5 for $T = 2000$ K, in Video 6 for $T = 2500$ K, in Video 7 for $T = 3000$ K, in Video 8 for $T = 3500$ K, and in Video 9 for $T = 4000$ K. Statistical-temperature averages taken during these runs indicate that the average temperature of a system prepared for $T = 500$ K changes to $\langle T \rangle = 480 \pm 17$ K, that of a system prepared for $T = 1000$ K changes to $\langle T \rangle = 1011 \pm 37$ K, that of a system prepared for $T = 1500$ K changes to $\langle T \rangle = 1466 \pm 48$ K, that of a system prepared for $T = 2000$ K changes to $\langle T \rangle = 2091 \pm 68$ K, that of a system prepared for $T = 2500$ K changes to $\langle T \rangle = 2622 \pm 79$ K, that of a system prepared for $T = 3000$ K changes to $\langle T \rangle = 2948 \pm 94$ K, that of a system prepared for $T = 3500$ K changes to $\langle T \rangle = 3518 \pm 111$ K, and that of a system prepared for $T = 4000$ K changes to $\langle T \rangle = 4204 \pm 142$ K in our *NVE* simulations. As stated above, the temperature to observe a specific process on a natural timescale is significantly lower than the simulation temperature in our time-limited study.

These MD simulations results suggest that the GO layers containing water molecules in the interlayer region remain intact below 2500 K. Nevertheless, these layers are flexible, and their deviation from planarity increases with temperature. With increasing temperature, liquid water turns to vapor, which exerts an increasing pressure on the

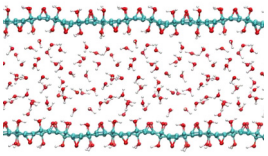

VIDEO 3. Microcanonical MD simulation of a hydrated-GO bilayer that is initially equilibrated at $T = 1000$ K.

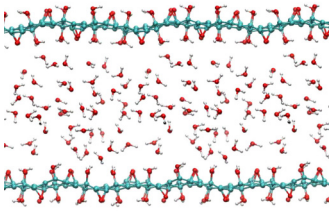

VIDEO 4. Microcanonical MD simulation of a hydrated-GO bilayer that is initially equilibrated at $T = 1500$ K.

containing layers and pushes them apart. At temperatures close to 4000 K, the GO layers are destroyed, whereas the water molecules appear to be unaffected.

Our finding that the graphitic backbone is the most-resilient part of the hydrated GO bilayer is well known, since bare graphene and graphite are known to survive temperatures up to approximately 3820 K [41].

B. Swelling at elevated temperatures

The effect of increasing water pressure on the interlayer distance d_{il} at elevated temperatures is shown in Fig. 3. For a given simulation temperature T, we plot the time evolution of the average interlayer distance $\langle d_{\mathrm{il}} \rangle (t)$, defined as an average separation d between C atoms in the top GO layer and the bottom GO layer in the direction normal to the plane of the bilayer. The error bars indicate the width of the distribution of d values across the unit cell. At a constant water pressure, which increases with temperature, we expect a constant acceleration, resulting in a parabolic dependence of the interlayer distance d_{il} on time t if we ignore the pressure drop during the short period considered. Quadratic fits to $\langle d_{\mathrm{il}} \rangle (t)$ are indicated by the dotted lines in Fig. 3. As expected, the acceleration of the interlayer separation, reflected in the harmonic coefficients, increases with increasing temperature due to the increasing water vapor pressure.

C. Coordination numbers at elevated temperatures

The simplest way to investigate the intactness of the graphitic backbone is a simple study of the distribution of the coordination number Z within the layer. In our study,

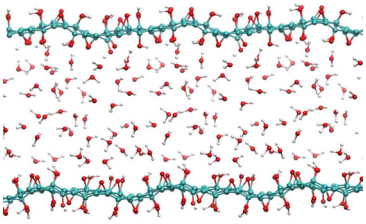

VIDEO 5. Microcanonical MD simulation of a hydrated-GO bilayer that is initially equilibrated at $T = 2000$ K.

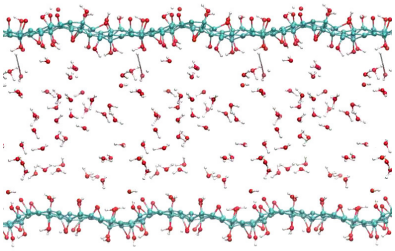

VIDEO 6. Microcanonical MD simulation of a hydrated-GO bilayer that is initially equilibrated at $T = 2500$ K.

we go through all 96 C atoms in the unit cell and count all other C atoms that are closer than 1.94 Å, the average between the nearest and the second-nearest distance in graphene, as nearest neighbors. This gives a discrete histogram for every simulation. Instead of an awkward comparison between seven histograms, we convolute the δ functions of different strength at integer values of Z by a Gaussian of FWHM of 0.5 and present the corresponding distribution $g(Z)$, with Z being a continuous variable now, in Fig. 4 for the different temperatures. Since the integral over $g(Z)$ is normalized to 1, the area of a peak at Z_i indicates the probability of any C atom having coordination number Z_i.

Our results show a single peak at $Z = 3$ for temperatures $T \lesssim 2000$ K, indicating that all carbon atoms maintain a graphenelike local environment with three nearest neighbors. At 2500 K we observe the emergence of a new peak at $Z = 2$, which becomes more prominent at 3000 K, indicating that some C—C bonds have been broken. $Z = 2$ carbon atoms are found at the edge of graphitic flakes or within linear chains. A new peak at $Z = 1$ emerges at $T \gtrsim 3500$ K, indicating C atoms at the end of a C chain. Finally, at $T \gtrsim 3500$ K, we observe the emergence of isolated C atoms with $Z = 0$ that are disconnected from the backbone.

D. Pair correlation function at elevated temperatures

A well-defined quantity to characterize the structure of the graphitic backbone is the pair correlation function

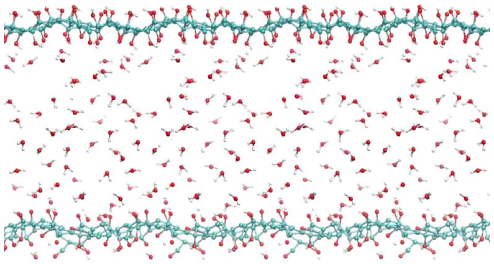

VIDEO 7. Microcanonical MD simulation of a hydrated-GO bilayer that is initially equilibrated at $T = 3000$ K.

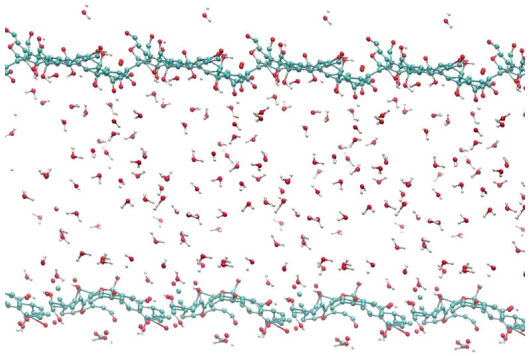

VIDEO 8. Microcanonical MD simulation of a hydrated-GO bilayer that is initially equilibrated at $T = 3500$ K.

$g_{\text{C-C}}(r)$, which indicates the probability of finding a C neighbor within a thin spherical shell of radius r around a C atom. Unlike the above-defined $g(Z)$, $g_{\text{C-C}}(r)$ can be observed by x-ray or electron-beam diffraction. In a perfect sheet of graphene frozen at $T = 0$, $g_{\text{C-C}}(r)$ consists of a series of δ functions, which are broadened and modified at higher temperatures. We display the time-averaged pair correlation function $\langle g_{\text{C-C}}(r)\rangle$ as a function of the distance r, obtained during our simulations, in Fig. 5 for MD runs at different simulation temperatures. Our results indicate that the shape of $g_{\text{C-C}}(r)$ does not change much from that of graphene for $T \lesssim 2000$ K. At higher temperatures, however, $\langle g_{\text{C-C}}(r)\rangle$ smoothes significantly, especially at larger interatomic distances.

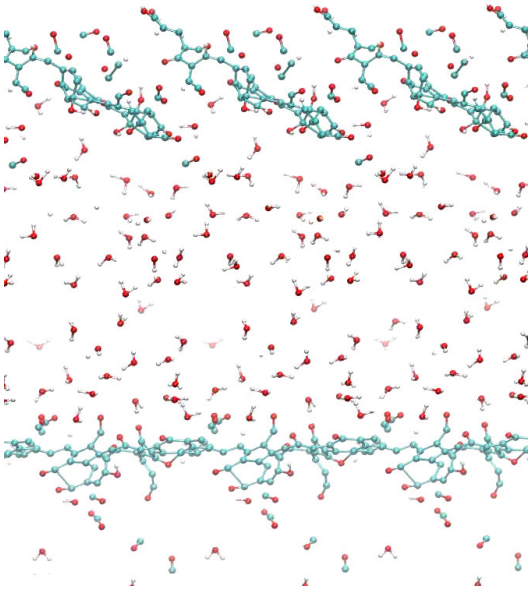

VIDEO 9. Microcanonical MD simulation of a hydrated-GO bilayer that is initially equilibrated at $T = 4000$ K.

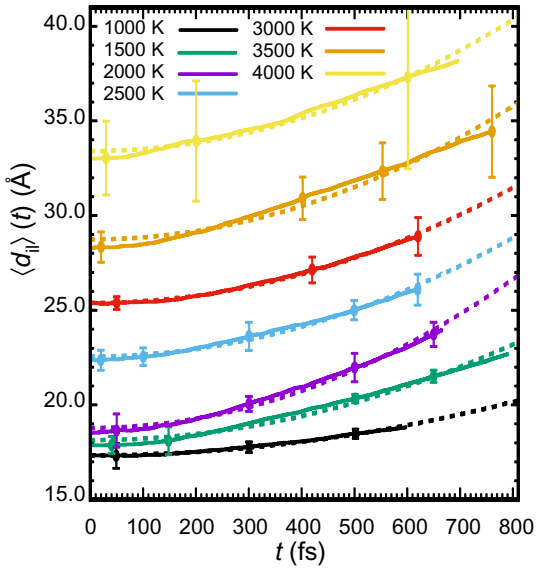

FIG. 3. Interlayer distance d_{il}, averaged across the unit cell, at different simulation temperatures T as a function of time t.

E. Changes in functional groups and H_2O at elevated temperatures

One of the important questions to which our study provides an answer is whether the epoxy-O and OH functional groups remain attached or whether they detach from the graphitic backbone before it thermally disintegrates. This information is important, since only functional groups that are chemically bonded to the substrate will weaken its structure locally and lower its melting temperature. A

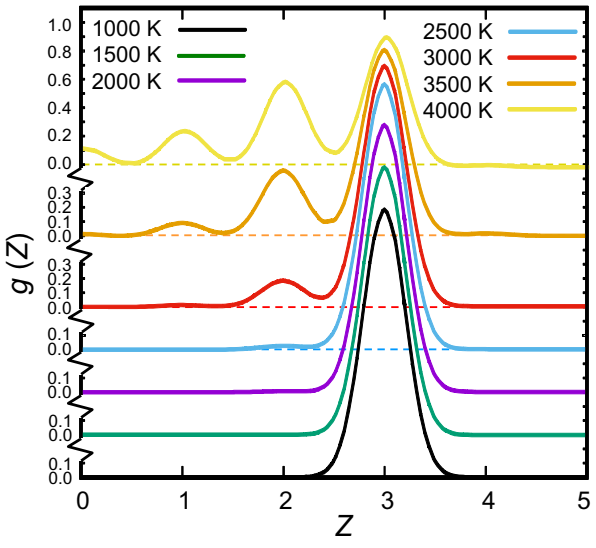

FIG. 4. Average distribution of coordination numbers Z within the C backbone of the bilayer as a function of the simulation temperature. For better comparison, the discrete distribution is convoluted by a Gaussian with a FWHM of 0.5.

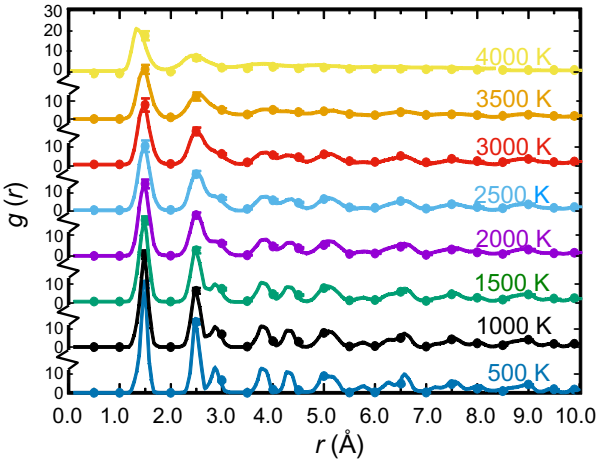

FIG. 5. Average C-C pair correlation function $\langle g(r)\rangle$ of the system as a function of the initial simulation temperature T, convoluted with a Gaussian with a FWHM of 0.1 Å.

useful guideline for the hierarchy of thermally activated processes is provided by comparing the relevant bond energies. These amount to 3.1–4.0 eV for a single C—C bond, 4.1 eV for a C—O bond, and 4.5 eV for an O—H bond [42]. Our results for the spread of interatomic distances in Fig. 6 are indeed consistent with the hierarchy of bond strengths and indicate that the functional groups generally stay chemisorbed to a defect-free graphitic backbone until its thermal destruction.

Exchange of hydrogen atoms between water molecules occurs even at 0 °C, as evidenced by investigations of D_2O/H_2O ice interfaces [43]. Earlier self-consistent charge-density functional tight-binding (SCC-DFTB) studies of "dry" GO indicate that hydrogen migration occurs in this material at ambient temperatures [34]. In our simulations we observe the first hydrogen hopping events at 2500 K, which represent both OH-water and OH–epoxy-O exchanges. As mentioned above, the high simulation temperature is necessitated by the limited duration of our thermally-accelerated MD study. With no time limit, the same processes will occur at much lower temperatures in nature.

Oxygen—carbon bonds survive up to even higher temperatures: OH groups remain attached to the graphitic layers up to 3000 K, followed by the detachment of epoxy-O groups at 3500 K. Some migration of oxygen atoms is observed at 2500 K and is discussed in the Appendix. SCC DFTB simulations reported oxygen-atom migration at 1323 K [34], which is close to the exfoliation temperature of GO in theoretical studies. Some results indicate agglomeration of oxygen-containing groups to form highly oxidized areas surrounded by nanodomains of pristine graphene [44] during GO aging. The small unit-cell size and limited simulation period do not allow us to judge if this process really occurs.

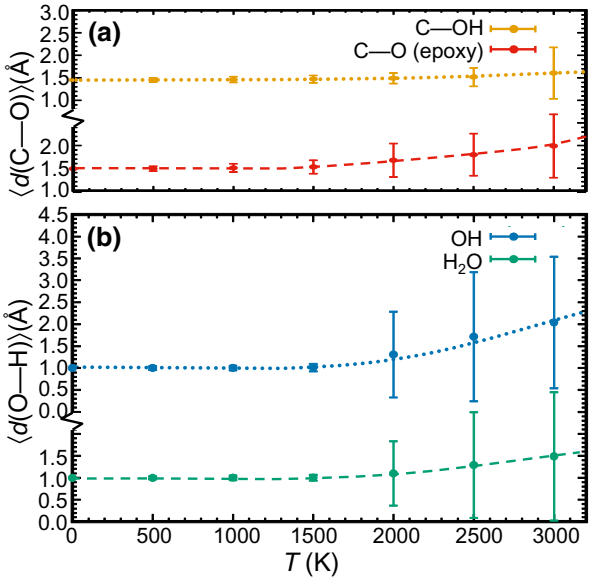

FIG. 6. (a) Average C—O distance $\langle d(\text{C—O})\rangle$ between oxygen atoms forming OH groups (dotted line) or epoxy bonds (dashed line) and their closest carbon neighbors as a function of the initial simulation temperature T. (b) Average O—H distance $\langle d(\text{O—H})\rangle$ between oxygen atoms forming OH groups (dotted line) or water molecules (dashed line) and their closest hydrogen neighbors as a function of T. Large error bars in the distribution indicate detachment of atoms or exchange of atoms with nearby molecules or radicals.

Epoxide groups were earlier shown to be of paramount importance for the thermal decomposition of GO sheets, since the C—C bond in an epoxy group breaks easier than a regular graphitic bond. According to DFT calculations, the barriers for this process are mostly less than 1.0 eV [45]. Aggregation of epoxy groups lower the barrier to approximately 0.6 eV. In the case of a linear arrangement of such defects, a crack in the carbon sheet is formed in a process dubbed "O-driven unzipping" [46]. We observe breaking of C—C-bonds in epoxy groups at a temperature as low as 3000 K in our simulations.

Our simulations indicate a total destruction of the GO backbone at $T \approx 4000$ K, accompanied by the detachment of small molecules as by-products. These by-products are dominated by carbon monoxide, in line with previously published results [34], as well as carbon dioxide and water. As during the thermal disintegration of other carbon allotropes [47], free-standing chains of several carbon atoms are formed, stabilized by their high entropy.

IV. DISCUSSION

As mentioned earlier, our attempt to provide atomic-scale insight into processes occurring in hydrated GO at elevated temperatures poses fundamental challenges and must be seen as only a first step toward obtaining microscopic understanding. The first limiting factor is the observation time. Activated processes, including oxidation and reduction of solid surfaces, occur on the timescale of seconds, whereas state-of-the-art *ab initio* calculations for unit cells containing a few hundred atoms may address only time intervals of approximately 10^{-12} s or less, requiring—as in our study—several months of CPU time on massively parallel supercomputers. We try to address this problem using thermally accelerated dynamics; namely, by exposing the system to an artificially increased external temperature. Even though this approach does not allow us to estimate at what temperature a particular process will occur in nature, it allows us to judge if specific reactions, such as migration of functional groups and their eventual detachment from the GO substrate, occur at lower temperatures than or at similar temperatures as the disintegration of the GO backbone that involves breaking of C—C bonds.

It is true that the *ab initio* approach is time-consuming. For this reason, the vast majority of atomistic MD simulations are based on parameterized force fields, which offer a higher degree of numerical efficiency and allow one to study the motion of several thousand atoms simultaneously. The CPU speed gain may be up to 3 orders of magnitude, but still falls short of the 12 orders of magnitude needed to observe relevant reactions. The drawback of parameterized force fields is their lack of universality and quantitative predictability, which may lead to incorrect conclusions. In particular, force fields optimized for bulk fluids need to be changed at interfaces and in situations where long-range electrostatic interactions play a nontrivial role [48,49]. In spite of its high computational demand, DFT is nominally free of parameters and independent of predefined assumptions. The approach used in this study has been validated, among other ways, by successfully predicting static and dynamic properties of liquid water [12], and should provide valuable information that should complement large-scale studies with parameterized force fields.

The second factor limiting our study is the arrangement of small graphitic flakes, functionalized by epoxy and hydroxy groups and separated by water, in realistic GO material that is lacking long-range order. Our study focuses on processes occurring on a pair of adjacent GO flakes separated by water, but ignores their finite size. Samples with different arrangements of GO flakes and different types of defects may behave very differently at high temperatures.

Even though the presence of water in the interlayer region does not affect the dynamics of the GO layers, H_2O molecules should in no way be considered as inert. Selected reactions we discuss in the Appendix indicate that hydrogen exchange between water molecules and epoxy or hydroxy functional groups is rather common at

elevated temperatures, still leaving water molecules among the stable products.

After revealing the strong points and limitations of our theoretical study, we must summarize what we have really learned. Many of our findings confirm conclusions based on chemical intuition. Water molecules remain intact up to the disintegration point of the GO backbone, initiated by breaking of C—C bonds near adsorbed functional groups. At high enough temperatures, liquid water turns into vapor that exerts a significant pressure on GO layers, separating them in a process known as swelling [50–52]. The presence of oxygen in functional groups is the microscopic reason for GO—unlike graphene and graphite—being hydrophilic. We find this to be the case in the Lerf-Klinowski model [38] of GO underlying our study, where the ratio of carbon to epoxy-O is 6. Functional groups may move across the GO substrate, often by intricate reactions involving adjacent water molecules. Still, epoxy and hydroxy groups do not desorb below the disintegration temperature of the GO backbone. At that point, these functional groups migrate to the graphitic edges exposed after fracture and terminate them.

We go to great lengths to automatically extract useful information from the vast number of atomic coordinate files collected during our MD simulations. Information obtained in this way includes statistical data about temperature fluctuations in Fig. 2, interlayer distances in Fig. 3, atomic coordination numbers in Fig. 4, the C-C pair correlation function in Fig. 5, and separation of functional groups from the substrate in Fig. 6. Our collected data for coordination numbers, pair correlation functions, and C—O and O—H distances clearly show that the structure of hydrated GO remains essentially unchanged up to the simulation temperature $T \approx 2000$ K. The only notable processes occurring below this temperature are GO swelling driven by water pressure, and buckling of the GO layers. Both of them show increasing amplitudes with increasing temperature.

We next subject our collected structural information to a data-mining analysis to search for unusual processes. We find that such unusual processes, which deserve the attribute of "chemical reactions," start occurring only at $T \approx 2000$ K. These include the fracture of the C—C bond, leading to undercoordinated carbon atoms with coordination number $Z < 3$ and hydrogen-exchange reactions, traced by the $\langle d(\text{C—O})\rangle$ distribution, which occur more frequently at high temperatures. Structural deterioration of the carbon substrate becomes particularly visible in the smoothing of the C-C pair correlation function $\langle g(r)\rangle$ at high temperatures.

Starting at $T \approx 2500$ K, we observe various reactions involving hydroxy groups and epoxy groups chemisorbed on GO layers and water molecules in the interlayer region. The reactions of interest, many of which are detailed in the Appendix, include hydrogen exchanges, interconversion between OH and epoxy groups, and the formation of peroxides, 1,3-epoxides, and monocoordinated oxygen atoms.

Our study of a defect-free model system, a hydrated-GO bilayer, does not address the reorientation of GO flakes in the presence of water that is free to escape through in-layer defects. Thus, dehydration and reduction of GO to rGO at high temperatures is beyond the scope of this study. Specific arrangements of GO flakes may block off compartments of different size within the system. Water contained in such compartments will exert pressure and eventually burst the containing structure at high-enough temperatures. This process, known as deflagration, may occur across a wide temperature range, as also evidenced in the experiment [53].

Our thermally accelerated MD simulations, while revealing commonly occurring reactions, do not allow us to estimate the temperature at which such reactions occur in nature on an unlimited timescale. As discussed earlier, the nominal simulation temperature may be seen as the upper limit of the expected temperature range, with a realistic value being approximately 200–2000 K lower. Still, we expect the sequence of thermal onsets of specific reactions to remain the same in our 1-ps simulations and, at reduced temperatures, under experimental conditions on a much longer timescale. For realistic temperature estimates, we may take recourse to what is known from the experiment.

High-temperature behavior of GO, specifically its thermal reduction, has been studied experimentally in a vast number of publications, with most attention devoted to Hummers GO. A comparative study of many GO samples produced in different ways revealed significant differences in their behavior [53,54]. Very impressive variations occur in the deflagration temperatures, ranging from 194 to 325 °C, with Hummers GO covering the lower end and Brodie GO covering the upper end of the temperature range. Most differences in behavior are caused by the size of GO flakes and functionalization on their faces and edges, flake arrangements within the sample, and the presence of water. Thermal decomposition of GO is an exothermic process, which is slowed down below the deflagration point by the evaporation of water [53].

Experimental data indicate that water escapes from GO above 100 °C [55], followed by exfoliation in the temperature range between 200 and 300 °C [53,56]. Along with loss of water [53], almost all oxygen-containing groups have been shown to disappear after heating to temperatures above 200 °C [57]. At these temperatures, GO has transformed to hydrophobic rGO, essentially graphitic carbon, with no swelling propensity [55].

Comparison between processes observed at a particular temperature and our thermally-accelerated-dynamics-simulation results indicates that the simulation temperature

of $T = 2500$ K roughly corresponds to the temperature range from 100 to 200 °C, which precedes formation of rGO.

At still higher temperatures, most interesting processes involve changes in the functional groups within rGO. Oxygen-containing groups decorating the faces are likely to migrate toward the reactive edges of disintegrating GO, where they survive as carboxyl and carbonyl groups up to the approximate temperature range 500–700 °C [55,58]. This finding is consistent with results of thermogravimetric analyses of GO samples, which were prepared by various methods [58] and displayed no weight loss above 600 °C [57,59]. Analysis of data obtained by electron-energy-loss spectroscopy and x-ray photoelectron spectroscopy for GO heated to different temperatures has revealed that epoxide groups disappear above 400 °C, whereas hydroxy groups remain present up to 1000 °C [60].

Further temperature increase leads to the detachment of other functional groups and fracture of the C—C bonds that initiates a gradual disintegration of GO. These processes occur at the simulation temperature of 4000 K, which should correspond roughly to $T \lesssim 1000$ K under realistic experimental conditions with no time constraints. Since processes at this stage are irreversible, this temperature range must be avoided during a thermal treatment of GO membranes.

Even though many experimental results related to the thermal decomposition of GO are controversial, there is general consensus about the major trends. Differences between published studies are likely related to inherent variations in the microstructure of GO samples produced by different techniques and subjected to different heat-treatment protocols [58].

V. SUMMARY AND CONCLUSIONS

In summary, we perform *ab initio* density-functional theory molecular dynamics simulations addressing thermally driven structural changes in a bilayer of hydrated graphite oxide in a vacuum. This rather artificial system is selected as a model to study microscopic details of the swelling and thermal decomposition of hydrated GO, which has been demonstrated to allow water permeation while rejecting solvated ions in the feed [11] when sandwiched in-between layers of carbon-nanotube buckypaper and carbon fabric for containment and mechanical strength [12]. To observe slow processes in the short time frame of the simulation, we artificially raise the system temperature in our thermally-accelerated MD studies of a perfect GO bilayer. Covering the temperature range [13] up to 4000 K, we find that water molecules in the interlayer region are rather decoupled from the GO layers and only marginally affect their behavior at moderate temperatures, except for increasing swelling by water vapor pressure. In the presence of nearby water molecules, some epoxy-O atoms move from their bridge to the on-top site, turning into radicals and changing the configuration of the connected carbon atom from sp^3 to sp^2. In a similar way, in the vicinity of water, hydrogen atoms may detach from adsorbed OH groups, converting them to epoxy groups. Both processes facilitate buckling and local fracture of the graphitic backbone above 2500 K. At higher temperatures, we observe the destruction of the graphitic backbone itself. Oxygen atoms in the functional groups migrate from the faces to the reactive exposed edges of the graphitic flakes. Depopulation of oxygen on the face of graphitic flakes turns GO into hydrophobic rGO, which is not subject to swelling.

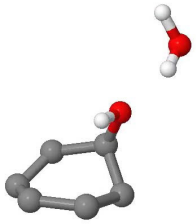

VIDEO 10. Interaction of a water molecule with an OH group attached to GO at the simulation temperature of 2000 K.

Combining knowledge contained in a vast number of experimental studies with the microscopic insight provided by our simulations, we find GO not only very promising for water treatment and desalination [11,12] but also thermally very stable. Thus, exposing GO membranes—in an inert-gas atmosphere containing water vapor—to temperatures below 300 °C or even higher may offer a viable alternative to chemical cleaning for removing biofouling residue.

ACKNOWLEDGMENTS

We appreciate the assistance of Barbod Naderi with the interpretation of atomic-level processes in the system. Computational resources for this study were provided by the Michigan State University High Performance Computing Center.

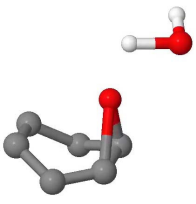

VIDEO 11. Interaction of a water molecule with an epoxy group attached to GO at the simulation temperature of 2500 K.

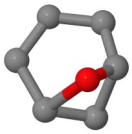

VIDEO 12. Formation of a 1,3-epoxide group and substrate destabilization at the simulation temperature of 2500 K.

APPENDIX

1. Atomic-scale reactions at the surface of hydrated GO

We subject the trajectory data of our MD simulations to an automated data-mining process to learn about interesting reactions that occur. These reactions are discussed in the following.

Video 10 demonstrates the attraction of a water molecule to a hydroxy group attached to GO, one of the reasons that GO becomes hydrophilic, at 2000 K. The dynamics of the rather-trivial reaction in this video, which depicts temporary attachment of H_2O to the oxygen in the hydroxy group, illustrates the role of hydrogen bonds, which are essential for the structure of ice and liquid water. These bonds constantly emerge and break in liquid water.

Video 11 depicts a very different process; namely, splitting of the C—O bond in an epoxide group at 2500 K, followed by a hydrogen transfer from a nearby H_2O molecule. The hydrogen transfer is expected on the basis of experimental data, which suggest that alkyl-OH groups are stronger acceptors of hydrogen bonds than water, while being comparable donors [61]. Thus, we may expect more-frequent formation of long-lasting hydrogen bonds with water being the donor and the OH group being the acceptor than the other way around. Epoxy groups, which have alkyl substituents, should then serve as even better hydrogen-bond acceptors. The process starts with a vibration in the three-membered ring constituting the epoxy group, during which one of the carbon—oxygen bonds breaks, releasing an estimated strain energy of 0.28 eV [62]. The singly coordinated oxygen atom then captures a hydrogen atom from an H_2O molecule. As a result, the initial epoxy group is converted to an OH group, whereas a water molecule turns into an OH anion.

Video 12 illustrates unusual epoxy-bond scenarios possible on a flexible substrate. During substrate vibrations, second neighbors in the graphene lattice may come close enough to bind with a "dangling" oxygen and thus form a 1,3-epoxide group. This structure appears to be rather stable at 2500 K, as also evidenced by its occurrence in nature; namely, as a part of cytotoxic triterpenes sodwanones I and W from marine sponge species [63,64]. Eventually, the strain energy is released by the breaking of a C—C bond in the substrate.

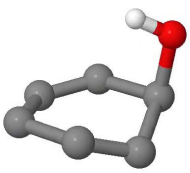

VIDEO 13. Hydroxy-group detachment from GO at the simulation temperature of 2500 K.

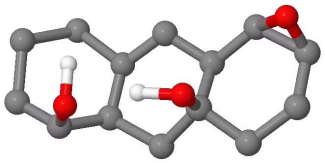

VIDEO 14. Chain reaction involving hydrogen transfers between epoxy and OH groups at the simulation temperature of 2500 K.

Video 13 illustrates the high stability of the bond between a hydroxy group and the carbon substrate. This bond eventually breaks at 2500 K in a process involving a low activation barrier of 0.27 eV according to DFT calculations [65].

Video 14 shows how different types of oxygen-containing groups may interconvert by hydrogen exchange at 2500 K. The lowest activation energy for such an exchange has been calculated to be 0.18 eV for OH and epoxy groups in adjacent 1,2-sites, but to increase significantly to 0.88 eV for 1,3-sites [65]. Our simulation illustrates two exchange events for 1,3-sites in a chain reaction involving hydrogen transfer. This process starts with an OH-OH-epoxy arrangement. After two exchange reactions, an epoxy-OH-OH configuration is formed. Evidently, the activation barriers are easily overcome at this high temperature, which results in frequent epoxy-OH conversions.

As seen in Video 15, a similar process involving hydrogen-exchange reactions may lead to the formation of singly coordinated oxygen atoms instead of epoxy groups, often facilitated by the puckering of the GO backbone at 2500 K. In the specific case visualized in the video, an epoxy group and a nearby singly coordinated oxygen may convert to a C-O-O-C peroxide structure. With its bond enthalpy below 2.07 eV [41], the peroxide bond is very weak and breaks easily, as seen further on in the video. Besides an intermittent fracture of the C—C bond near

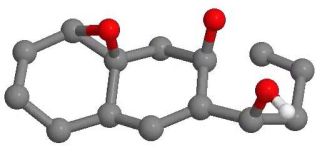

VIDEO 15. Hydrogen exchange followed by a C-O-O-C peroxy-group formation at the simulation temperature of 2500 K.

the functional groups, we do not observe serious structural damage to the GO backbone at 2500 K.

[1] J. Kucera, ed., *Desalination: Water from water* (Wiley, 2014).

[2] Y. Cohen, R. Semiat, and A. Rahardianto, A perspective on reverse osmosis water desalination: Quest for sustainability, AIChE J. **63**, 1771 (2017).

[3] R. Epsztein, R. M. DuChanois, C. L. Ritt, A. Noy, and M. Elimelech, Towards single-species selectivity of membranes with subnanometre pores, Nat. Nano **15**, 426 (2020).

[4] S. K. Patel, C. L. Ritt, A. Deshmukh, Z. Wang, M. Qin, R. Epsztein, and M. Elimelech, The relative insignificance of advanced materials in enhancing the energy efficiency of desalination technologies, Energy Environ. Sci. **13**, 1694 (2020).

[5] J. R. Werber, C. O. Osuji, and M. Elimelech, Materials for next-generation desalination and water purification membranes, Nat. Rev. Mater. **1**, 16018 (2016).

[6] J. Kucera, Biofouling of polyamide membranes: Fouling mechanisms, current mitigation and cleaning strategies, and future prospects, Membranes **9**, 111 (2019).

[7] N. Porcelli and S. Judd, Chemical cleaning of potable water membranes: A review, Sep. Purif. Technol. **71**, 137 (2010).

[8] E. M. Deemer, T. Capt, O. Owoseni, T. Akter, and W. S. Walker, Hypochlorite resistant graphene oxide incorporated ultrafiltration membranes with high sustainable flux, Ind. Eng. Chem. Res. **58**, 11964 (2019).

[9] M. Elimelech and W. A. Phillip, The future of seawater desalination: Energy, technology, and the environment, Science **333**, 712 (2011).

[10] M. W. Shahzad, M. Burhan, D. Ybyraiymkul, and K. C. Ng, Desalination processes' efficiency and future roadmap, Entropy **21**, 84 (2019).

[11] H.-P. Boehm, A. Clauss, and U. Hofmann, Graphite oxide and its membrane properties, J. Chim. Phys. **58**, 141 (1961).

[12] D. Tománek and A. Kyrylchuk, Designing an All-Carbon Membrane for Water Desalination, Phys. Rev. Appl. **12**, 024054 (2019).

[13] The need for an artificial temperature increase in thermally accelerated MD simulations is discussed in Sec. II.

[14] B. C. Brodie, XIII. On the atomic weight of graphite, Phil. Trans. Roy. Soc. (London) **149**, 249 (1859).

[15] W. S. Hummers and R. E. Offeman, Preparation of graphitic oxide, J. Am. Chem. Soc. **80**, 1339 (1958).

[16] A. Boretti, S. Al-Zubaidy, M. Vaclavikova, M. Al-Abri, S. Castelletto, and S. Mikhalovsky, Outlook for graphene-based desalination membranes, npj Clean Water **1**, 5 (2018).

[17] Z. Wang, C. Ma, C. Xu, S. A. Sinquefield, M. L. Shofner, and S. Nair, Graphene oxide nanofiltration membranes for desalination under realistic conditions, Nat. Sustainability **4**, 402 (2021).

[18] U. Hofmann, A. Frenzel, and E. Csalán, Die Konstitution der Graphitsäure und ihre Reaktionen, Justus Liebigs Ann. Chem. **510**, 1 (1934).

[19] A. Akbari, P. Sheath, S. T. Martin, D. B. Shinde, M. Shaibani, P. C. Banerjee, R. Tkacz, D. Bhattacharyya, and M. Majumder, Large-area graphene-based nanofiltration membranes by shear alignment of discotic nematic liquid crystals of graphene oxide, Nat. Commun. **7**, 10891 (2016).

[20] J. Zhang, Z. Xu, M. Shan, B. Zhou, Y. Li, B. Li, J. Niu, and X. Qian, Synergetic effects of oxidized carbon nanotubes and graphene oxide on fouling control and anti-fouling mechanism of polyvinylidene fluoride ultrafiltration membranes, J. Memb. Sci. **448**, 81 (2013).

[21] M. Hu, S. Zheng, and B. Mi, Organic fouling of graphene oxide membranes and its implications for membrane fouling control in engineered osmosis, Environ. Sci. Technol. **50**, 685 (2016).

[22] X. Huang, K. L. Marsh, B. T. McVerry, E. M. Hoek, and R. B. Kaner, Low-fouling antibacterial reverse osmosis membranes via surface grafting of graphene oxide, ACS Appl. Mater. Interf. **8**, 14334 (2016).

[23] J. L. Han, X. Xia, Y. Tao, H. Yun, Y. N. Hou, C. W. Zhao, Q. Luo, H. Y. Cheng, and A. J. Wang, Shielding membrane surface carboxyl groups by covalent-binding graphene oxide to improve anti-fouling property and the simultaneous promotion of flux, Wat. Res. **102**, 619 (2016).

[24] M. H.-O. Rashid and S. F. Ralph, Carbon nanotube membranes: Synthesis, properties, and future filtration applications, Nanomaterials **7**, 99 (2017).

[25] J. Ai, L. Yang, G. Liao, H. Xia, and F. Xiao, Applications of graphene oxide blended poly(vinylidene fluoride) membranes for the treatment of organic matters and its membrane fouling investigation, Appl. Surf. Sci. **455**, 502 (2018).

[26] D. H. Seo, S. Pineda, Y. C. Woo, M. Xie, A. T. Murdock, E. Y. M. Ang, Y. Jiao, M. J. Park, S. I. Lim, M. Lawn, F. F. Borghi, Z. J. Han, S. Gray, G. Millar, A. Du, H. K. Shon, T. Y. Ng, and K. Ostrikov, Anti-fouling graphene-based membranes for effective water desalination, Nat. Commun. **9**, 683 (2018).

[27] R. E. Pérez-Roa, M. A. Anderson, D. Rittschof, C. G. Hunt, and D. R. Noguera, Involvement of reactive oxygen species in the electrochemical inhibition of barnacle (*Amphibalanus amphitrite*) settlement, Biofouling **25**, 563 (2009).

[28] X. Lu, X. Feng, X. Zhang, M. Chukwu, C. O. Osuji, and M. Elimelech, Fabrication of desalination membrane with enhanced microbial resistance through vertical alignment of graphene oxide, Environ. Sci. Technol. Lett. **5**, 614 (2018).

[29] K. Ho, Y. Teow, A. Mohammad, W. Ang, and P. Lee, Development of graphene oxide (GO)/multi-walled carbon nanotubes (MWCNTs) nanocomposite conductive membranes for electrically enhanced fouling mitigation, J. Memb. Sci. **552**, 189 (2018).

[30] A. Quandt, A. Kyrylchuk, G. Seifert, and D. Tománek, Liquid Flow through Defective Layered Membranes: A Phenomenological Description, Phys. Rev. Appl. **14**, 044038 (2020).

[31] C. L. Ritt, J. R. Werber, A. Deshmukh, and E. Menachem, Monte Carlo simulations of framework defects in layered two-dimensional nanomaterial desalination membranes: Implications for permeability and selectivity, Environ. Sci. Technol. **53**, 6214 (2019).

[32] B. Corry, Designing carbon nanotube membranes for efficient water desalination, J. Phys. Chem. B **112**, 1427 (2008).

[33] A. Kyrylchuk and D. Tománek, Flow of polar and nonpolar liquids through nanotubes: A computational study, Phys. Rev. Mater. **5**, 076001 (2021).

[34] J. T. Paci, T. Belytschko, and G. C. Schatz, Computational studies of the structure, behavior upon heating, and mechanical properties of graphite oxide, J. Phys. Chem. C **111**, 18099 (2007).

[35] E. Artacho, E. Anglada, O. Dieguez, J. D. Gale, A. Garcia, J. Junquera, R. M. Martin, P. Ordejon, J. M. Pruneda, D. Sanchez-Portal, and J. M. Soler, The SIESTA method; developments and applicability, J. Phys. Cond. Mat. **20**, 064208 (2008).

[36] J. P. Perdew, K. Burke, and M. Ernzerhof, Generalized Gradient Approximation Made Simple, Phys. Rev. Lett. **77**, 3865 (1996).

[37] N. Troullier and J. L. Martins, Efficient pseudopotentials for plane-wave calculations, Phys. Rev. B **43**, 1993 (1991).

[38] A. Lerf, H. He, M. Forster, and J. Klinowski, Structure of graphite oxide revisited, J. Phys. Chem. B **102**, 4477 (1998).

[39] G. Cicero, J. C. Grossman, E. Schwegler, F. Gygi, and G. Galli, Water confined in nanotubes and between graphene sheets: A first principle study, J. Am. Chem. Soc. **130**, 1871 (2008).

[40] A. Ambrosetti and P. L. Silvestrelli, Adsorption of rare-gas atoms and water on graphite and graphene by van der Waals-corrected density functional theory, J. Phys. Chem. C **115**, 3695 (2011).

[41] R. C. Weast, ed., *CRC Handbook of Chemistry and Physics*, 62nd ed. (CRC Press, Boca Raton, FL, USA, 1982).

[42] R. C. Weast, ed., *CRC Handbook of Chemistry and Physics*, 67th ed. (CRC Press, Boca Raton, FL, USA, 1986).

[43] R. Drori, M. Holmes-Cerfon, B. Kahr, R. V. Kohn, and M. D. Ward, Dynamics and unsteady morphologies at ice interfaces driven by D_2O-H_2O exchange, Proc. Natl. Acad. Sci. **114**, 11627 (2017).

[44] S. Zhou and A. Bongiorno, Density functional theory modeling of multilayer "epitaxial" graphene oxide, Acc. Chem. Res. **47**, 3331 (2014).

[45] T. Sun and S. Fabris, Mechanisms for oxidative unzipping and cutting of graphene, Nano Lett. **12**, 17 (2012).

[46] J.-L. Li, K. N. Kudin, M. J. McAllister, R. K. Prud'homme, I. A. Aksay, and R. Car, Oxygen-Driven Unzipping of Graphitic Materials, Phys. Rev. Lett. **96**, 176101 (2006).

[47] S. G. Kim and D. Tomanek, Melting the Fullerenes: A Molecular Dynamics Study, Phys. Rev. Lett. **72**, 2418 (1994).

[48] M. H. Köhler, J. R. Bordin, C. F. de Matos, and M. C. Barbosa, Water in nanotubes: The surface effect, Chem. Eng. Sci. **203**, 54 (2019).

[49] R. P. Misra and D. Blankschtein, Insights on the role of many-body polarization effects in the wetting of graphitic surfaces by water, J. Phys. Chem. C **121**, 28166 (2017).

[50] A. V. Talyzin, V. L. Solozhenko, O. O. Kurakevych, T. Szabó, I. Dékány, A. Kurnosov, and V. Dmitriev, Colossal pressure-induced lattice expansion of graphite oxide in the presence of water, Angew. Chem. Int. Ed. **47**, 8268 (2008).

[51] A. Talyzin, S. Luzan, T. Szabó, D. Chernyshev, and V. Dmitriev, Temperature dependent structural breathing of hydrated graphite oxide in H_2O, Carbon **49**, 1894 (2011).

[52] A. Iakunkov, N. Boulanger, A. Nordenström, and A. V. Talyzin, Swelling pressures of graphite oxide and graphene oxide membranes in water and ethanol, Adv. Mater. Interf. **8**, 2100552 (2021).

[53] H.-P. Boehm and W. Scholz, Der "Verpuffungspunkt" des Graphitoxids, Z. Anorg. Allg. Chem. **335**, 74 (1965).

[54] P. Feicht, R. Siegel, H. Thurn, J. W. Neubauer, M. Seuss, T. Szabó, A. V. Talyzin, C. E. Halbig, S. Eigler, D. A. Kunz, A. Fery, G. Papastavrou, J. Senker, and J. Breu, Systematic evaluation of different types of graphene oxide in respect to variations in their in-plane modulus, Carbon **114**, 700 (2017).

[55] Alexandr V. Talyzin, private communication.

[56] S. You, S. M. Luzan, T. Szabó, and A. V. Talyzin, Effect of synthesis method on solvation and exfoliation of graphite oxide, Carbon **52**, 171 (2013).

[57] Z. Hu, Y. Chen, Q. Hou, R. Yin, F. Liu, and H. Chen, Characterization of graphite oxide after heat treatment, New J. Chem. **36**, 1373 (2012).

[58] E. M. Deemer, P. K. Paul, F. S. Manciu, C. E. Botez, D. R. Hodges, Z. Landis, T. Akter, E. Castro, and R. R. Chianelli, Consequence of oxidation method on graphene oxide produced with different size graphite precursors, Mater. Sci. Eng. B **224**, 150 (2017).

[59] F. Farivar, P. L. Yap, K. Hassan, T. T. Tung, D. N. Tran, A. J. Pollard, and D. Losic, Unlocking thermogravimetric analysis (TGA) in the fight against "fake graphene" materials, Carbon **179**, 505 (2021).

[60] D. D'Angelo, C. Bongiorno, M. Amato, I. Deretzis, A. La Magna, E. Fazio, and S. Scalese, Oxygen functionalities evolution in thermally treated graphene oxide featured by EELS and DFT calculations, J. Phys. Chem. C **121**, 5408 (2017).

[61] M. H. Abraham, P. P. Duce, D. V. Prior, D. G. Barratt, J. J. Morris, and P. J. Taylor, Hydrogen bonding. Part 9. Solute proton donor and proton acceptor scales for use in drug design, J. Chem. Soc. Perkin Trans. 2 **25**, 1355 (1989).

[62] D. L. Whalen, Mechanisms of hydrolysis and rearrangements of epoxides, Adv. Phys. Org. Chem. **40**, 247 (2005).

[63] J. Dai, J. A. Fishback, Y.-D. Zhou, and D. G. Nagle, Sodwanone and yardenone triterpenes from a South African species of the marine sponge *Axinella* inhibit hypoxia-inducible factor-1 (HIF-1) activation in both breast and prostate tumor cells, J. Nat. Prod. **69**, 1715 (2006).

[64] A. Rudi, I. Goldberg, Z. Stein, Y. Kashman, Y. Benayahu, M. Schleyer, and M. D. G. Gravalos, Sodwanones G, H, and I, new cytotoxic triterpenes from a marine sponge, J. Nat. Prod. **58**, 1702 (1995).

[65] N. Lu, D. Yin, Z. Li, and J. Yang, Structure of graphene oxide: Thermodynamics versus kinetics, J. Phys. Chem. C **115**, 11991 (2011).